JACS
JOURNAL OF THE AMERICAN CHEMICAL SOCIETY
Article
pubs.acs.org/JACS

Modular Design of Self-Assembling Peptide-Based Nanotubes

Natasha C. Burgess,[†,‡] Thomas H. Sharp,[§,▽] Franziska Thomas,[†,▽] Christopher W. Wood,[†,∥] Andrew R. Thomson,[†] Nathan R. Zaccai,[∥] R. Leo Brady,[∥] Louise C. Serpell,[⊥] and Derek N. Woolfson*[,†,∥,#]

[†]School of Chemistry, University of Bristol, Cantock's Close, Bristol, BS8 1TS, United Kingdom
[‡]Bristol Centre for Functional Nanomaterials, University of Bristol, Tyndall Avenue, Bristol, BS8 1FD, United Kingdom
[§]Section Electron Microscopy, Department of Molecular Cell Biology, Leiden University Medical Center, Leiden, The Netherlands
[∥]School of Biochemistry, University of Bristol, Medical Sciences Building, University Walk, Bristol, BS8 1TD, United Kingdom
[⊥]School of Life Sciences, University of Sussex, Falmer, Brighton, East Sussex, BN1 9QG, United Kingdom
[#]BrisSynBio, University of Bristol, Life Sciences Building, Tyndall Avenue, Bristol, BS8 1TQ, United Kingdom

Supporting Information

ABSTRACT: An ability to design peptide-based nanotubes (PNTs) rationally with defined and mutable internal channels would advance understanding of peptide self-assembly, and present new biomaterials for nanotechnology and medicine. PNTs have been made from Fmoc dipeptides, cyclic peptides, and lock-washer helical bundles. Here we show that blunt-ended α-helical barrels, that is, preassembled bundles of α-helices with central channels, can be used as building blocks for PNTs. This approach is general and systematic, and uses a set of de novo helical bundles as standards. One of these bundles, a hexameric α-helical barrel, assembles into highly ordered PNTs, for which we have determined a structure by combining cryo-transmission electron microscopy, X-ray fiber diffraction, and model building. The structure reveals that the overall symmetry of the peptide module plays a critical role in ripening and ordering of the supramolecular assembly. PNTs based on pentameric, hexameric, and heptameric α-helical barrels sequester hydrophobic dye within their lumens.

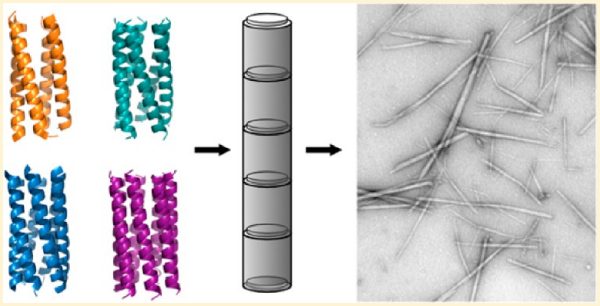

INTRODUCTION

The rational design and controlled assembly of peptide-based fibers is now well established.[1,2] Such structures are being developed for applications in nanotechnology and in medicine, including the templated assembly of hybrid materials,[3] and as scaffolds for tissue engineering.[4] Extending these capabilities to peptide nanotubes (PNTs) would advance our control over biomaterials design considerably,[4] and open routes to biomaterials with high aspect ratios and large internal surfaces. If the sizes and chemistries of the cavities could also be engineered, the resulting structures would have potential additional applications such as the storage and controlled release of small molecules;[4,5] as catalysts, with the incorporation of active sites into the channels;[6] and for the controlled deposition of ultrathin metallic wires of prescribed diameter.[7]

Among other examples, the assembly of PNTs has been demonstrated using short Fmoc-dipeptides,[7] and cyclic peptides of alternating D- and L-amino acids.[8,9] Of direct relevance to this report, several groups have employed sticky ended α-helical coiled coils to make peptide-based fibers.[10−12] In many of these cases, coiled-coil dimers, trimers, and occasionally tetramers are used, which results in largely solid fibers.[13] Extending this to the use of α-helical barrels,[14] that is, coiled-coil pentamers and above that have central, solvent-accessible lumens (Figure 1a and b), would open additional routes to PNTs. Indeed, several groups have succeeded in making peptide-based fibers and nanotubes from such building blocks: Potekhin et al. take advantage of the repetitive nature of coiled-coil sequences to deliver a pentamer with an axial stagger;[15] Montclare and co-workers have redesigned a natural pentamer, COMP;[16] and Conticello's laboratory have remodeled a known spiral-like heptamer, GCN4-pAA.[17] There are clear advantages of these systems, notably their availability and simplicity. However, they are solutions to the challenge of design and assembly of PNTs that employ bespoke building blocks. To expand possibilities in this area, we sought a general and modular method for producing PNTs from chemically accessible and standard building blocks, which could be altered predictably to access a range of PNTs with channels of predetermined internal diameter and chemistry.

Our starting point was our own basis set, or toolkit of stably and discretely folded de novo coiled coils.[18] The toolkit was generated using known sequence-to-structure relationships for coiled-coil assembly, and its components have been characterized in detail both in solution and by X-ray protein crystallography.

Received: April 17, 2015
Published: July 28, 2015

DOI: 10.1021/jacs.5b03973
J. Am. Chem. Soc. 2015, 137, 10554−10562

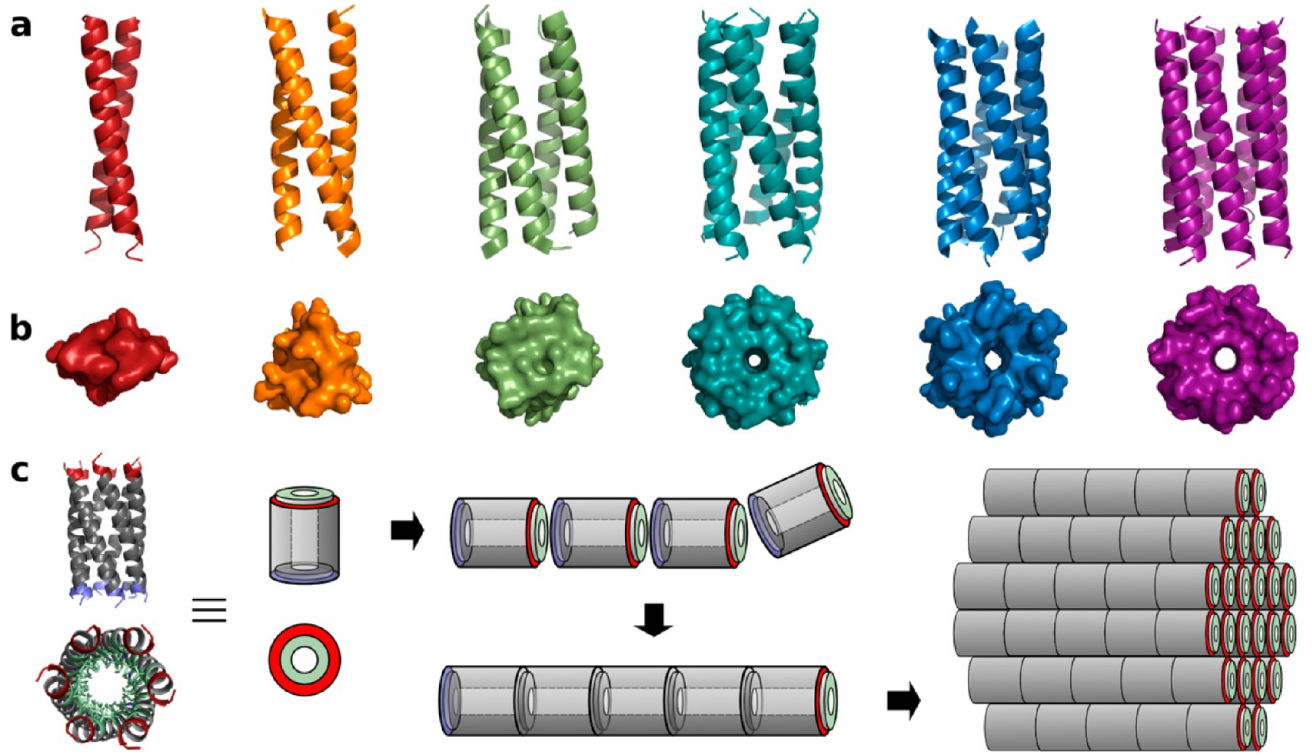

Figure 1. X-ray crystal structures of the coiled-coil toolkit, and depiction of a general mode of assembly of peptide fibers and PNTs. (a) Ribbon diagrams for coiled-coil structures: CC-Di (red; PDB code 4DZM), CC-Tri (orange; 4DZL), CC-Tet (green; 3R4A), CC-Pent (turquoise; 4PN8), CC-Hex (blue; 3R3K), and CC-Hept (purple; 4PNA). (b) Orthogonal views of space-filling models for the structures shown in panel (a). (c) Proposed general mode of end-to-end assembly of blunt-ended coiled-coil building blocks to form fibers and broadened PNTs. In the cartoons of panel (c), which are based on CC-Hex-T (Table 1), the positively and negatively charged side chains at the *N*- and *C*-termini of the peptide are indicated by blue and red coloring, and the exposed hydrophobic side chains are colored green. It is these side chains that were designed to promote hydrophobic and electrostatic interactions and to drive fiber assembly similar to Conticello and co-workers.[17]

The toolkit includes coiled-coil homodimers through tetramers, and heterodimers and a heterotrimer.[19−21] Recently, we have expanded the toolkit to include more-complex coiled coils, including pentamers, hexamers, and a heptamer, which are the lowest-order α-helical barrels (Figure 1a and b).[22,23] The peptide assemblies of the toolkit are generally stable to small numbers of mutations, and can be used as robust building blocks in a range of contexts.[6,24,25]

Here we demonstrate a general design strategy for creating peptide-based fibers and nanotubes using the toolkit (Figure 1c). After applying our methodology, all but two of the toolkit peptides form linear supramolecular assemblies. In addition, one of the variants, a hexamer designated CC-Hex-T, can be induced to form highly ordered and porous fibrous materials. For this material, detailed diffraction and imaging methods reveal square-packed bundles of CC-Hex-T-based nanotubes, and indicate that the geometry of the building block plays a key role in the formation of ordered assemblies.

RESULTS AND DISCUSSION

Design of Peptide Modules. From previous studies, and under a wide variety of conditions that we have explored, none of the components from the coiled-coil toolkit readily assemble beyond the designed and experimentally defined oligomeric state, and we have not observed fiber formation for any of these peptides.[6,22,23] We assume that this is prevented by the terminal capping sequences, which should destabilize any end-to-end association of the coiled-coil assemblies. Therefore, for the study described herein, we modified the termini of the designs to test if fiber or PNT assembly could be promoted (Table 1).

As a starting point for our designed modules, peptide sequences were taken from the central, coiled-coil, heptad repeats known to give specific oligomer states in the toolkit peptides from dimer through to heptamer.[18,23] Charged residues (E or K) were placed at the C-termini of the sequences to complement oppositely charged side chains in the N-terminal repeats; patches of hydrophobic core were left exposed near the N-termini (I or L residues at the **a** and **d** positions of the heptad sequence repeat (**abcdefg**), Table 1). This was done to give minimal, rather than large-scale changes to the toolkit peptides. The resulting sequences were synthesized with free amino and carboxy termini. In these ways, we aimed to promote end-to-end assembly of the classical coiled coils (i.e., oligomer states 2−4) or of the α-helical barrels (oligomer states 5−7) through hydrophobic and electrostatic interactions. In turn, we postulated that this should lead to the formation of extended fibers or tubes, respectively, in which the helices and heptad repeats are contiguous that is, that they read through from one oligomer to the next.

The Majority of the Peptide Modules Form Fibrous Assemblies. As judged by negative-stain transmission electron microscopy (TEM, Figure 2), all of the redesigned peptides, except for CC-Di-F and CC-Tet-F, assembled spontaneously and immediately upon dissolution in aqueous buffer. Fiber formation was the prevailing result and occurred at relatively low peptide concentrations (~40 μM) compared with other fiber-forming systems[11] (Supporting Information Figure S1). This in itself is telling, as we know that the discrete α-helical

DOI: 10.1021/jacs.5b03973
J. Am. Chem. Soc. 2015, 137, 10554−10562

Table 1. Sequences for the "Parent" de Novo Coiled-Coil Toolkit Peptides, Followed by Those Adapted from These to Form Fibers and Nanotubes, with the Latter Distinguished in Bold[a]

Peptide	Sequence and Heptad Repeat
	g abcdefg abcdefg abcdefg abcdefg abc
CC-pIL-I17N	Ac-G E IAALKQE IAALKKE NAALKWE IAALKQ GYY-NH_2
CC-Di-F	**H- IAALKQE IAALKKE NAALKWE IAALKQE -OH**
CC-pII	Ac-G E IAAIKQE IAAIKKE IAAIKWE IAAIKQ GYG-NH_2
CC-Tri-F	**H- IAAIKQE IAAIKKE IAAIKWE IAAIKQE -OH**
CC-pLI	Ac-G E LAAIKQE LAAIKKE LAAIKWE LAAIKQ GAG-NH_2
CC-Tet-F	**H- LAAIKQE LAAIKKE LAAIKWE LAAIKQE -OH**
CC-Tet2	Ac-G NILQE VKNILKE VKNILWE VKNILQE VK G-NH_2
CC-Tet2-F	**H- NILQE VKNILKE VKNILWE VKNILQE VK -OH**
CC-Pent	Ac-G KIEQI LQKIEKI LQKIEWI LQKIEQI LQ G-NH_2
CC-Pent-T	**H- IEQI LQKIEKI LQKIEWI LQKIEQI LQK -OH**
CC-Hex	Ac-G E LKAIAQE LKAIAKE LKAIAWE LKAIAQ GAG-NH_2
CC-Hex-T	**H- LKAIAQE LKAIAKE LKAIAWE LKAIAQE -OH**
CC-Hex2	Ac-G EIAKS LKEIAKS LKEIAWS LKEIAKS LK G-NH_2
CC-Hex2-T	**H- EIAQS LKEIAKS LKEIAWS LKEIAQS LK -OH**
CC-Hex3	Ac-G EIAQS IKEIAKS IKEIAWS IKEIAQS IK G-NH_2
CC-Hex3-T	**H- EIAQS IKEIAKS IKEIAWS IKEIAQS IK -OH**
CC-Hex-IL	Ac-G E IKALAQE IKALAKE IKALAWE IKALAQ G-NH_2
CC-HexIL-T	**H- IKALAQE IKALAKE IKALAWE IKALAQE -OH**
CC-Hept	Ac-G EIAQA LKEIAKA LKEIAWA LKEIAQA LK G-NH_2
CC-Hept-T	**H- EIAQA LKEIAKA LKEIAWA LKEIAQA LK -OH**

[a]Peptides were synthesized as C-terminal acids. MALDI-TOF and HPLC data for pure peptides are presented in the Supporting Information (Figure S2). The components are denominated "CC-oligomer state", e.g., CC-Hex for the hexamer with six α-helices; and, in the text, with suffices -F (for CC-Di → Tet) or -T (CC-Pent → Hept), which signifies that the structures should form fibers (F) and tubes (T), respectively.

barrels are long-lived (i.e., kinetically stable) structures;[6] thus, it is reasonable to assume that these discrete states are the blocks for fiber assembly. Consistent with this, circular dichroism (CD) spectroscopy indicated that assembly occurred without gross changes to the peptide α-helical secondary structure (Supporting Information Figure S3). For all fiber-forming peptides, we prepared dried stalks and recorded X-ray fiber diffraction (XRD) patterns (Supporting Information Figure S4 and Table S1). Encouragingly, these patterns were similar to each other. Moreover, they were fully consistent with previously described patterns for α-helical fibers in which the α-helices are aligned parallel to the long axis of the fiber.[10,26] Specifically, our data sets all showed meridional reflections in the range 0.48−0.51 nm, which arise from the α-helical repeat of the polypeptide backbones tilted with respect to the long axis of the fiber, as expected for canonical coiled coils;[27] plus, series of equatorial reflections, which arise from the packing of α-helical bundles orthogonal to this axis. Therefore, these patterns are entirely consistent with bundles of helical fibrils aligned parallel with the long axis of the fibers, and, thus, with the coiled-coil units arranged end-to-end.

The redesigned dimer, CC-Di-F, could not be induced to assemble further either by increasing peptide concentration, or by altering the solution conditions. We attribute this to the small exposed surface at the ends of a dimer, which limits the platform from which fibers can be built. This supports the widely followed contention that sticky ends are needed for fiber assembly with such small constructs.[10,11] CC-Tri-F did form fibers, although these were shorter and thinner than those observed for the higher-order coiled-coil assemblies (Figure 2 and Supporting Information Table S2). Given this observation, and even though fiber formation is a complex process, we were surprised that CC-Tet-F did not form fibers under any conditions tested. Therefore, we tested another tetramer-forming sequence, CC-Tet2, discovered in our recent expansion of the toolkit.[23] We redesigned this to promote fiber assembly as described above to give CC-Tet2-F (Table 1). This peptide did form fibers (Figure 2b, Supporting Information Table S2 and Figure S3).

Thermal Unfolding and Annealing the Supramolecular Assemblies. Summarizing the above, except for the dimer and one of the tetramers, all of the redesigned, blunt-ended coiled-coil modules assemble into various fibrous morphologies. However, all were thickened compared with those expected for

DOI: 10.1021/jacs.5b03973
J. Am. Chem. Soc. 2015, 137, 10554−10562

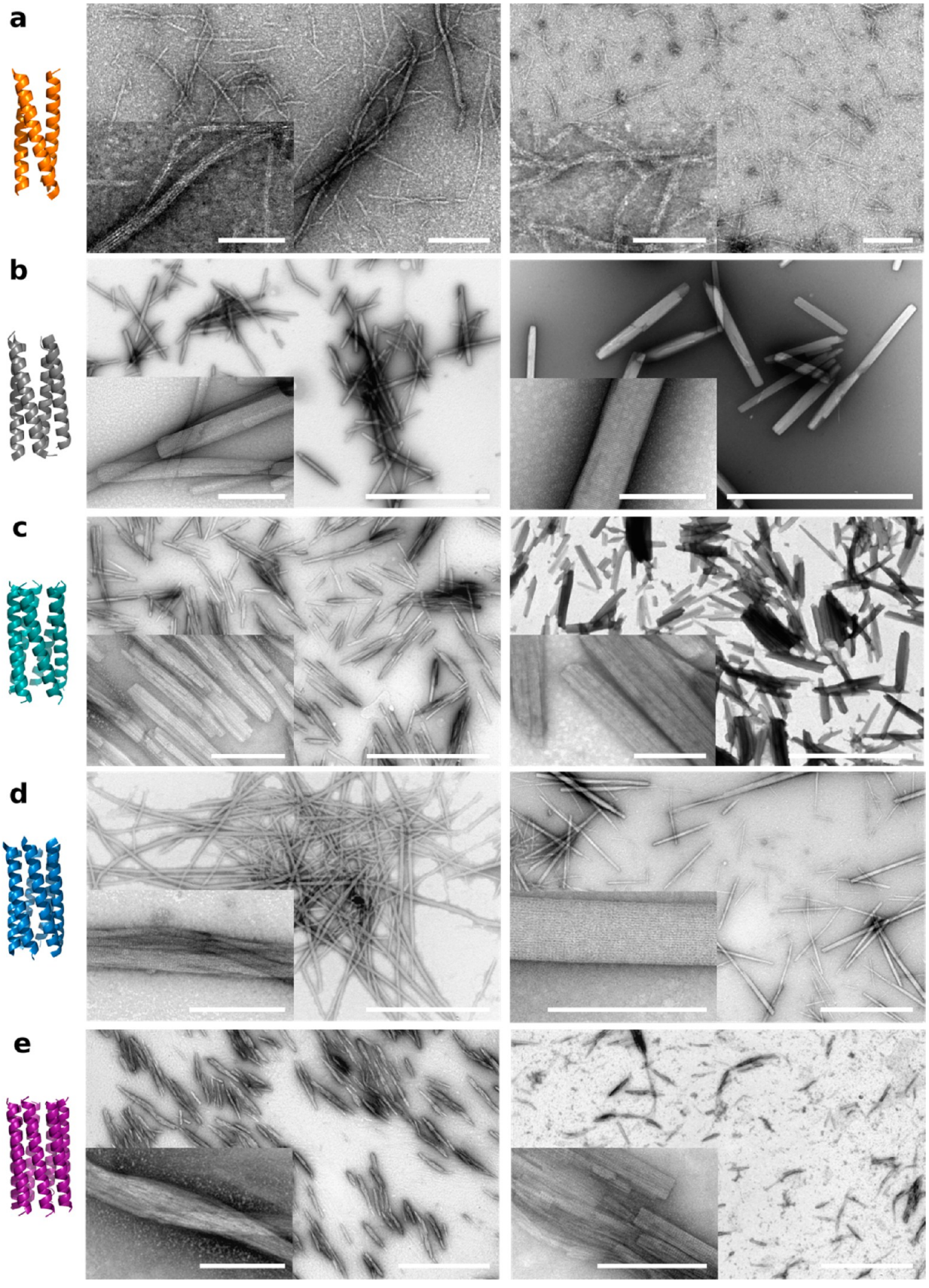

Figure 2. Negative-stain transmission electron micrographs of coiled-coil peptide fibers. Left: X-ray crystal structures (available for all but CC-Tet2, panel b). Middle: Images for freshly prepared samples assembled at 20 °C. Right: Images after heating from 5 to 95 °C over 180 min, followed by cooling to 25 °C over 20 min. (a) CC-Tri-F. (b) CC-Tet2-F (CC-Tet crystal structure shown in gray). (c) CC-Pent-T. (d) CC-Hex-T. (e) CC-Hept-T. Scale bars: (a) 200 nm, inset = 100 nm; (b–e) 2000 nm, inset = 200 nm. Conditions: 100 μM peptide, phosphate-buffered saline (PBS), pH 7.4.

DOI: 10.1021/jacs.5b03973
J. Am. Chem. Soc. 2015, 137, 10554–10562

simple, linearly extended, single chains (fibrils) of the building blocks (Figure 2, Supporting Information Table S2 and Figure S5). Such ripening is common in α-helical fibrous systems, and arises because symmetric assembly of identical building blocks creates patches on the fibril surfaces that foster fibril−fibril interactions and lead to thick-fiber formation.[13,28] Given the spontaneous and rapid assembly of the fibers, it is possible that these states are kinetically trapped structures, rather than global thermodynamic minima. Therefore, we followed the effect of temperature on spontaneously formed fibers by CD spectroscopy and then by TEM (Supporting Information Figure S3 and Figure 2). The assemblies showed different responses.

When followed by CD spectroscopy, only CC-Tri-F gave a complete and sigmoidal thermal denaturation curve consistent with cooperative disassembly and unfolding of the thin fibril and discrete peptide assemblies. The other peptides showed either little response to temperature, incomplete transitions, or complex behavior (Supporting Information Figure S3). Thus, except for CC-Tri-F, we assumed that none of the fibrous peptide assemblies sampled completely unfolded states of the peptides. TEM revealed shortened and less-well ordered fibers for heat-treated CC-Tri-F compared with the spontaneously formed structures (Figure 2a). Heat treatment of CC-Tet2-F led to a transition at 40 °C, and, upon cooling, a growth in fiber diameter from 60−65 nm to 130−135 nm (Supporting Information Figure S5), but with no dramatic change in visible surface order, that is, the suprastructure of the fibers (Figure 2b). The fibers formed by CC-Pent-T at 20 °C changed into broad, sheetlike structures when heated above 40 °C followed by cooling (Figure 2c and Supporting Information Figure S6). Similar treatment of CC-Hept-T formed a mixture of precipitate and short, but ordered fibers (Figure 2e).

By contrast, heating and cooling of the spontaneously formed CC-Hex-T fibers produced highly ordered structures of ∼70 nm in diameter with clear and reproducible ultrastructure (Figures 2d and 3, and Supporting Information Figure S7). This effect was apparent in both the CD spectroscopy and TEM images. The former showed a slight initial loss of signal up to 50 °C; followed by a first transition at 55−65 °C, indicating an increase in α-helicity; and then the onset of a thermal unfolding transition above 70 °C (Supporting Information Figure S3). After cooling, a repeat melting curve indicated more-stable species, and repeat cooling and melting showed no further changes in structure (Supporting Information Figure S8). On this basis, subsequently we incubated CC-Hex-T samples at 65 °C for 1 h in aqueous buffer, before cooling them slowly for further analysis of what we term *annealed fibers*.

Ultrastructure and Organization in Annealed CC-Hex-T Fibers. Negatively stained TEM images of heat-treated CC-Hex-T fibers revealed regular striations both laterally and longitudinally (Figure 2d). Fourier transforms of these showed uniform spacings of 4.3 and ∼3 nm, respectively (Supporting Information Figure S9), which are closely similar to the dimensions of CC-Hex from the X-ray crystal structure (4.3 × 3.4 × 3.4 nm), and with the longer dimension (4.3 nm) corresponding to the projected length of the 28-residue α-helices (vide infra).

We used XRD to compare the spontaneously formed and annealed fibers (Figure 3a and b). These both showed reflections on the meridian at 0.51 nm (M) arising from the α-helical repeat of the polypeptide backbones[27] along the axis of the fibers, and thus confirmed end-to-end assembly of the coiled-coil modules as designed. There were no indications of

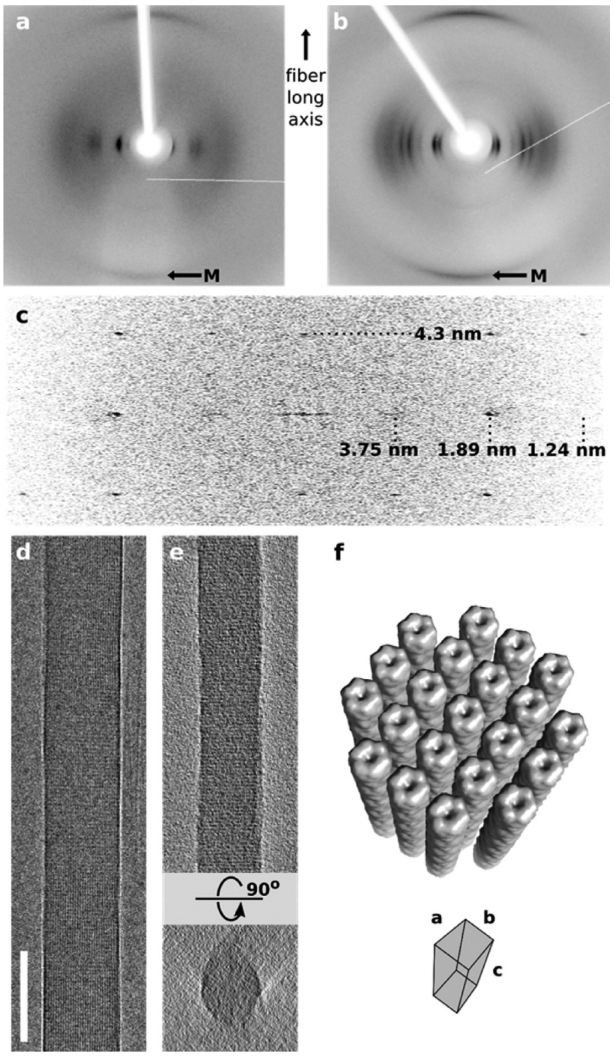

Figure 3. Secondary and quaternary structures of CC-Hex-T fibers from X-ray fiber diffraction (XRD) and cryo-TEM. (a) XRD pattern for the CC-Hex-T fibers assembled at room temperature in PBS, pH 7.4 (with solvent exchanged to water for the measurements), orientated with the meridional axis (fiber long axis) vertical. M = 0.508 nm. (b) XRD pattern for the annealed CC-Hex-T fibers. M = 0.506 nm (full list of reflections in Supporting Information Table S3). (c) Indexed and annotated Fourier transform from a cryo-TEM image. (d) Typical cryo-TEM image of annealed CC-Hex-T fibers, scale bar = 100 nm. (e) Cryo-TEM tomographic slice of a CC-Hex-T fiber (incubated with aurothiomalate and the image shown is an average of 50 slices to aid contrast) showing their approximately cylindrical nature. (f) Square-packed model for CC-Hex-T fibers for $a = b$ = 3.75 nm and c = 4.3 nm as described in the text.

reflections consistent with β-sheet or other secondary/tertiary structure arrangements in either sample. The annealed fibers showed many more reflections (Figure 3a and b and Supporting Information Table S3). This is consistent with increased order in comparison to the spontaneously formed samples. However, these could not be indexed to one definitive packing arrangement. This is possibly due to drying the samples, which is required to give aligned fibers for XRD. Therefore, we turned to cryo-transmission electron microscopy (cryo-TEM) to visualize the annealed fibers in a near-native, hydrated state without stain (Figure 3d). This revealed ultrastructure similar to that observed by negative-stain TEM. These features must reflect directly the underlying structure of the

DOI: 10.1021/jacs.5b03973
J. Am. Chem. Soc. 2015, 137, 10554−10562

fibers. Fourier transforms of the cryo-electron micrographs indicated clear and regularly spaced reflections (Figure 3c and Supporting Information Table S4), which we interpret below. In addition, cryo-TEM tomograms showed cylindrical and solid fibers and, with increased contrast using cryo-negative stain, striations running through the structures (Figure 3e).

Combining our data, we propose the following model for the assembly and structure of the CC-Hex-T paracrystalline fibers.

Taking the ultrastructure features in turn: the lateral striations, that is, those that run across a fiber perpendicular to its long axis, were spaced at 4.3 nm. This is approximately the length expected for a 28-residue coiled-coil bundle (28 × 0.15 nm = 4.2 nm), as observed in CC-Hex.[22] Hence, CC-Hex-T units are most likely arrayed end-to-end to form fibrils, and side-by-side to make fibers. Furthermore, no layer lines other than orders of 4.3 nm were apparent from along the length of the structures (Figure 3c). This absence of layer lines without zero-order Bessel functions is intriguing and indicates that the peptide length and the overall coiled-coil pitch in this case must be related by an integer value, and that this must be 6, the order of the rotation axis (Supporting Information Figure S10).[29] Thus, the predicted pitch is 6 × 4.3 nm =25.8 nm, which is experimentally indistinguishable from that predicted from the X-ray crystal structure of CC-Hex (25.88 nm).[22] Therefore, in the annealed but still hydrated fibers, we posit that the CC-Hex-T units form 6_1 superhelices, that is, precisely equivalent to the coiled-coil superhelical pitch, which pack unperturbed within the matured fibers.

We note that there is an alternative model in which the helices of the bundles are completely straight and themselves aligned with the long axis of the α-helical barrel, and hence with the long axis of the α-helical fibrils and fibers. In other words, the coiled coil may not supercoil. This would also account for the absence of peaks other than that at 4.3 nm from the peptide modules. However, we believe that this is extremely unlikely for two reasons: First, coiled coils that are based on heptad repeats are invariably supercoiled, as this is a consequence of Crick's model.[27] Second, CC-Hex has a very clear left-handed supercoil, Figure 1a, which is evident from the 0.51 nm meridional reflections (M) in the XRD of both the spontaneously formed and annealed fiber samples of CC-Hex-T (Figure 3a and b). In the absence of a coiled-coil supercoil, the latter reflections would be at or close to 0.54 nm.

The longitudinal striations on the fibers observed by TEM and quantified by Fourier transform (Figure 3c, Supporting Information Table S4), provide information on the side-by-side packing of CC-Hex-T units and nanotube fibrils. Row lines were observed at 3.68, 2.63, 1.88, 1.70, 1.33, 1.24, and 0.94 nm, which are in the ratio of $1/\sqrt{1}:1/\sqrt{2}:1/\sqrt{4}:1/\sqrt{5}:1/\sqrt{8}:1/\sqrt{9}:1/\sqrt{16}$. This is consistent with square packing of hexameric coiled-coil rods (fibrils) with primitive tetragonal unit-cell dimensions $a = b = 3.75$ nm and $c = 4.3$ nm.

From the above dimensions and using the coiled-coil modeling program, CCBuilder,[30] we generated an in silico model of arrayed CC-Hex-T units. This model revealed spaces between the CC-Hex-T-based fibrils in the hydrated state. It stands to reason that these cavities might collapse upon drying, which may explain why we could not index the XRD data unequivocally, but that we could for the cryo-TEM data (Supporting Information Tables S3 and S4). The EM diffraction data do not have sufficient resolution to determine whether the array comprises parallel or antiparallel fibrils, or a mixture of the two (paracrystalline array).

CC-Hex Variants That Break Packing Symmetry Do Not Lead to Highly Organized Fibers. It stands to reason that hexameric building blocks should suit fiber formation and maturation, as the C_6 symmetry is the highest possible to build periodic crystals. Indeed, fibers formed by CC-Hex-T were longer and more regular than those made by CC-Pent-T or CC-Hept-T (Figure 2). Moreover, CC-Hex-T was the only α-helical-barrel to give paracrystalline fibers when annealed. We argue that this results from the simple, integer relationship between the length of the CC-Hex building block and its overall coiled-coil pitch (vide supra, Supporting Information Figure S11).

To investigate this further, three other hexamers were selected from our toolkit. Namely, CC-Hex2 and CC-Hex3,[23] which are blunt-ended assemblies like CC-Hex (Figure 4a and b); and a staggered hexamer, CC-HexIL, in which the sixth α-helix is slipped by one heptad relative to the first (Figure 4c). The geometric and coiled-coil parameters (length, radius, channel size, and coiled-coil pitch) are all different from those for CC-Hex (Supporting Information Tables S5 and S6). The peptides have all been characterized fully in solution, with no observed association into fibrous forms. Each peptide was redesigned to promote fiber assembly (Table 1), and, indeed, all three formed fibers spontaneously at 20 °C (Figure 4). However, none of the resulting fibers showed high-order ultrastructure upon heating and cooling as seen with CC-Hex-T. Given that the oligomer state of the four peptides is the same, and that one of the sequences, CC-HexIL-T, is closely similar to that for CC-Hex-T (Table 1), this suggests that subtle effects determine if highly ordered fibers can be formed or not. As none of the variants have coiled-coil superhelical pitches that match simple multiples of the building-block length, we posit that it is this feature that dictates this level of assembly (Supporting Information Table S5).

Accessibility of the Internal Channel of CC-Hex-T. Finally, we tested if the lumen of the original CC-Hex-based nanotubes was accessible to small molecules using a fluorescence-binding assay and the linear hydrophobic dye 1,6-diphenylhexatriene (DPH). This is an environment-sensitive dye that does not fluoresce in water, but fluoresces strongly at 455 nm in hydrophobic surroundings.[31,32] Since the channel of CC-Hex-T is lined with hydrophobic residues, and is of the appropriate size to harbor the dye, we hypothesized that encapsulation of DPH should result in strong fluorescence. Indeed, equilibration of increasing concentrations of CC-Hex-T with DPH revealed a steady increase in fluorescence and saturation binding (Figure 5).

To establish that the observed fluorescence resulted from DPH encapsulation directly within the hydrophobic channel of CC-Hex-T, and not from nonspecific inclusions into the peptide array, we performed control experiments with discrete CC-Tet2; fibrous, but nontubular CC-Tet2-F; and with discrete, unmodified CC-Hex. DPH fluorescence was not observed for discrete CC-Tet2 or its fibrous form, CC-Tet2-F (Figure 5a). These controls demonstrate that more than just coiled-coil or fibrous structures per se are required for dye binding. We note that there is a possible caveat to these experiments: nonspecific binding of fluorophore to the surfaces of the fibrous materials may not be registered as any resulting fluorescence may be quenched by water. However, given the highly polar character of the outer surfaces of the α-helical bundles and barrels, we feel that such binding modes are unlikely.

DOI: 10.1021/jacs.5b03973
J. Am. Chem. Soc. 2015, 137, 10554−10562

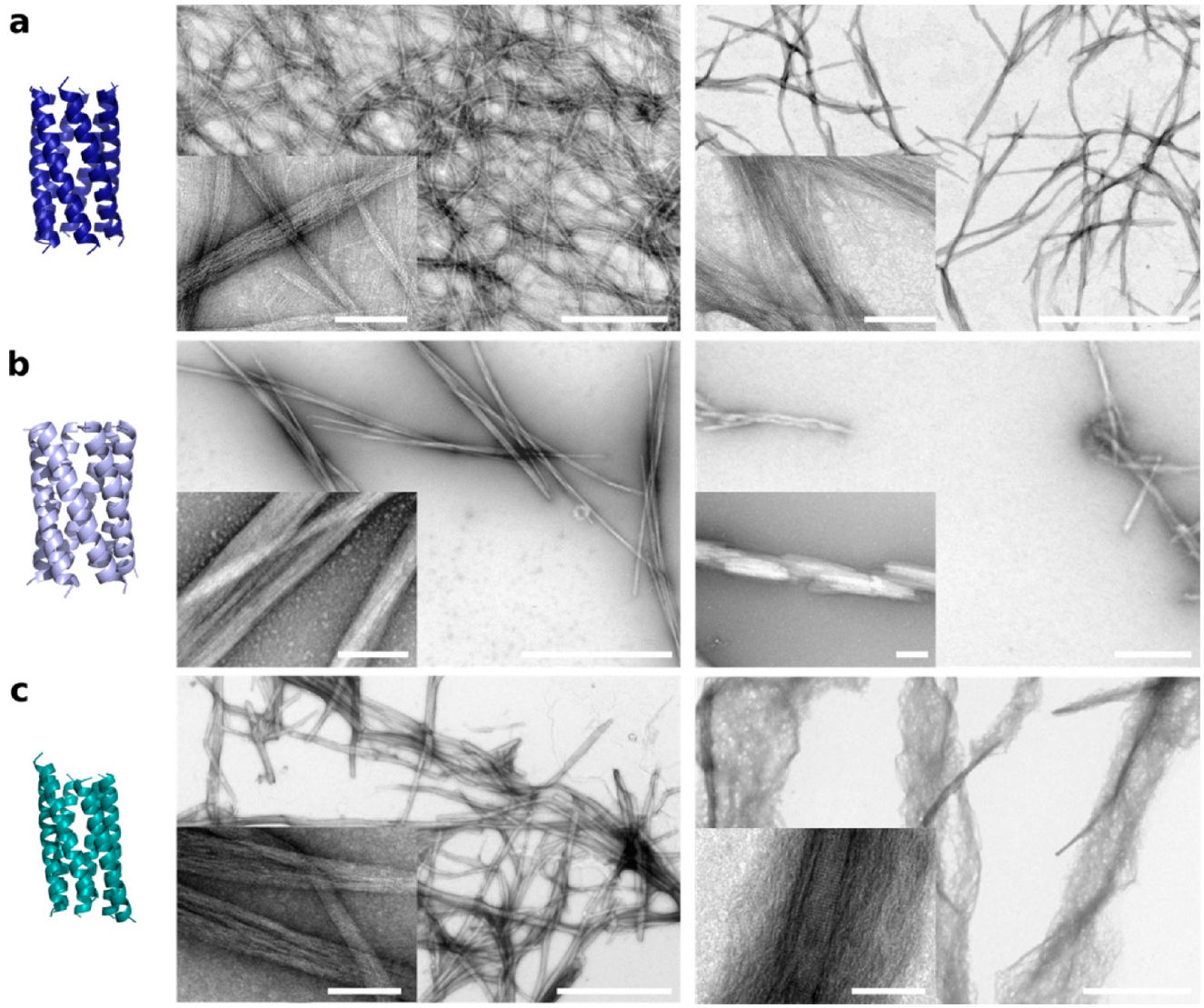

Figure 4. Fibers formed by the alternative hexameric α-helical-barrel building blocks. (a) CC-Hex2 (PDB code 4PN9). (b) CC-Hex3 (4PNB). (c) CC-Hex-IL (4H8G). Left: Ribbon diagrams of the X-ray crystal structures. Middle: TEM images of fibers spontaneously formed from 100 μM peptide, PBS, pH 7.4, 20 °C. Right: Fibers resulting from heating from 5 to 95 °C over 180 min and then cooled to 25 °C over 20 min. Scale bars = 1000 nm; inset scale bar = 100 nm.

As a positive control, fluorescence was observed with soluble CC-Hex (Figure 5a), and this fitted to a single-site binding model with a dissociation constant of 29.2 μM (Figure 5b). Interestingly, comparison of the saturation-binding curves for the discrete (CC-Hex) and tubular forms (CC-Hex-T) of the hexamer indicated tighter binding of DPH to the PNTs. Figure 5b. However, quantification of this type of binding to supramolecular assemblies is difficult, and was not attempted, because for such systems there will likely be multiple and possibly cooperative binding events within the contiguous lumen of the PNTs. Encouraged by these findings, however, we also performed DPH binding experiments with CC-Tri-F, CC-Pent-T, and CC-Hept-T. Although the measurements were complicated by scattering effects, the results strongly support DPH encapsulation in the tubular assemblies, CC-Pent-T and CC-Hept-T, whereas no evidence for DPH binding was observed in the case of CC-Tri-F (Figure 5c and d). Together, these experiments demonstrate the binding of a linear, hydrophobic molecule within the lumens of α-helical-barrel-based nanotubes and discrete α-helical barrels.

CONCLUSION

In summary, we have demonstrated that prefolded, de novo α-helical coiled-coils and barrels can be used as standard building blocks for the assembly of peptide fibers and nanotubes with high aspect ratios. The blunt-ended mode of assembly that we demonstrate appears to be general, other than that for dimeric building blocks, which may be a special case,[10,33] as we show that trimeric through heptameric assemblies can all be used. Others have made similar observations for a small number of isolated cases.[11,16,17] This assembly mode removes the necessity for using, or creating lock-washer or sticky ended building blocks,[10,17] which are serendipitous discoveries or bespoke designs rather than general, rationally engineered building blocks. As a result, we have generated a range of peptide fibers and nanotubes. For the latter, we have shown that the internal lumens are accessible to, and provide binding sites for a hydrophobic dye. We propose that these building blocks, the ability to engineer them, the demonstrated encapsulation, and the general mode of assembly provide a firm

DOI: 10.1021/jacs.5b03973
J. Am. Chem. Soc. 2015, 137, 10554−10562

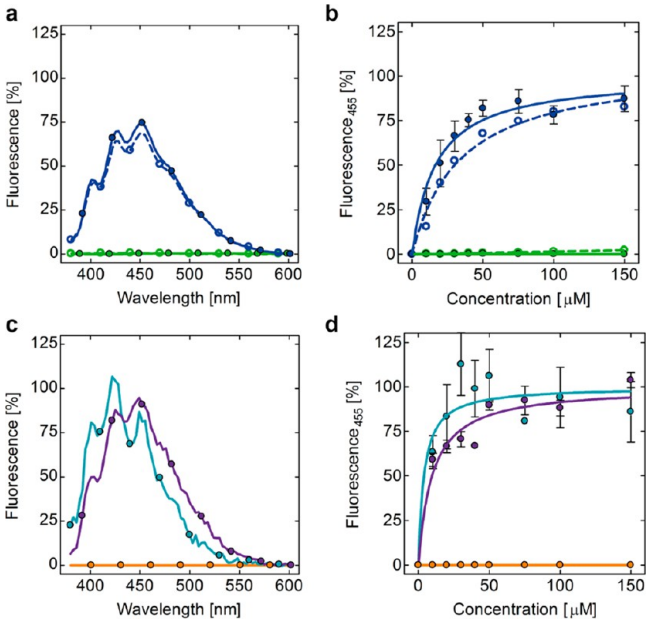

Figure 5. Accessibility of the channel of CC-Pent-T, CC-Hex-T, and CC-Hept-T to the hydrophobic dye 1,6-diphenylhexatriene (DPH). (a and c) Fluorescence spectra of 1 μM DPH (λ_{ex} = 350 nm) in the presence of 50 μM peptide. (a) CC-Hex-T (blue, solid discs and continuous line), CC-Hex (blue, open circles and dashed line); CC-Tet2-F (green, solid discs and continuous line), and CC-Tet2 (green, open discs and dashed line). (c) CC-Tri-F (orange, solid discs and continuous line), CC-Pent-T (turquoise, solid discs and continuous line), and CC-Hept-T (purple, solid discs and continuous line). (b and d) Saturation binding at 455 nm of 1 μM DPH to varying concentrations of peptide. (b) CC-Hex-T, CC-Hex (K_d = 29.2 ± 2.4 μM), CC-Tet2-F, CC-Tet2. (d) CC-Tri-F, CC-Pent-T, and CC-Hept-T. Key: same as that for panels (a) and (c). Saturation binding curves were fitted to a hyperbolic function to facilitate qualitative comparisons. Data were normalized to Y_{max} (maximum Y value) obtained from fitting. Experiments were performed in PBS at pH 7.4 with 1 μM DPH and peptide concentrations ranging from 10–150 μM, allowing samples to equilibrate for 2 h before measurements.

basis for the rational design of peptide nanotubes that span the nano-to-meso scales. Moreover, they present opportunities for introducing functions within chemical and spatially defined lumens of PNTs via the substitution of modified building blocks with altered internal chemistries.[6]

Interestingly, the CC-Hex-T building block forms fibrous assemblies that can be annealed to give ordered arrays of peptide nanotubes, whereas the other building blocks do not. We argue that the symmetry and specifically the superhelical pitch of the coiled-coil is the key determinant of whether a particular building block will form such arrays. CC-Hex-T forms the highly symmetric structures because it has C_6 symmetry, and a pitch equivalent to an exact multiple of peptide-unit lengths to give a 6_1 superhelix. The superhelices then pack unperturbed on a square lattice to form the highly ordered fibrous assemblies of peptide nanotubes. By contrast, in the well-characterized self-assembled peptide fiber (SAF) system highly ordered fibers result from remodeling of the component dimeric coiled-coil units to give an altered pitch compatible with 3_1 superhelices and hexagonal packing, corresponding to a 12% compression of the coiled-coil pitch.[13] We propose that where the peptide fibers and nanotubes formed by other α-helical coiled-coil and barrel peptides explored herein do not form highly ordered arrays it is because: (1) their symmetries are incompatible with the required highly symmetric fibril–fibril packing; and (2) the building blocks are less flexible or compressible and are not readily remodeled. This understanding should guide biomaterials designers to pick building blocks from nature, or to make them de novo, to render highly ordered peptide- and protein-based fibers or nanotubes on demand.

EXPERIMENTAL SECTION

Materials and Methods. Unless otherwise stated, biophysical measurements were performed in phosphate-buffered saline, pH 7.4 (PBS: 10 mM phosphate, 137 mM NaCl, 2.7 mM KCl). Peptide concentrations were determined by UV absorbance (ε_{280}(Trp) = 5690 mol^{-1} cm^{-1}) using a NanoDrop 2000 spectrophotometer (ThermoScientific).

Synthesis. Peptides were synthesized on a 0.1 mmol scale using standard Fmoc-protocols for microwave-assisted solid-phase peptide synthesis (CEM Liberty Synthesizer, CEM corp.). Crude peptides were cleaved from the resin by agitation with a cleavage solution of 95% trifluoroacetic acid (TFA)/5% triisopropylsilane/5% water for ~3 h. The TFA mix was separated from the solid resin and evaporated to <5 mL, and the peptide precipitated by addition of ~45 mL of ice-cold diethyl ether. Suspensions were centrifuged, the supernatants discarded, and peptides were then redissolved in 1:1 water/acetonitrile and freeze-dried to give the crude product.

Purification. Crude peptides were purified using reverse phase high performance liquid chromatography (HPLC, JASCO (UK) Ltd.) fitted with a Phenomenex C18 column (150 × 10 mm) and water +0.1% TFA (buffer A) and acetonitrile +0.1% TFA (buffer B) as the mobile phases. Peptides were typically eluted with a linear gradient of 30% − 70% buffer B, 3 mL min^{-1} flow rate, over 35 min. Peptide masses were measured by MALDI-TOF mass spectrometry (Applied Biosystems 4700 Series Proteomics Analyzer) from a 2,5-dihydroxybenzoic acid matrix. Fraction purity was checked by analytical HPLC C18 column (Phenomenex 100 Å column (100 × 4.6 mm)). Chromatograms were monitored at 220 and 280 nm wavelengths. Pure peptide fractions were pooled and freeze-dried. MALDI-TOF and HPLC data for all peptides presented in this paper are shown in Supporting Information Figure S2.

Circular Dichroism (CD) Spectroscopy. CD measurements were taken using JASCO J-815 or J-810 spectrometer fitted with a Peltier temperature controller. Spectra were taken in a 1 mm quartz cuvette (100 μM peptide, PBS) at 20 °C using 1 nm interval, 1 nm bandwidth and 16 s response time. Thermal denaturation experiments were taken from 5–90 °C following the signal at 222 nm (40 °C h^{-1} ramp, 1 nm bandwidth) unless otherwise stated. Ellipticities (deg) were collected, baseline corrected and converted to mean residual ellipticities (MRE).

Transmission Electron Microscopy (TEM). The following electron microscopes were used: a JEOL JEM 1200 (tungsten filament, 120 kV) for negatively stained images, and a Tecnai T20 (with a LaB_6 filament, 200 kV) and Tecnai F20 (FEG, 200 kV) were used for TEM at cryogenic temperatures (cryo-TEM) and electron tomography on negatively stained samples. Continuous-film carbon-coated copper grids (Electron Microscopy Sciences) were used for negative staining (200 square-mesh grids), and lacey carbon copper grids for cryo-TEM (300 square-mesh). Peptide fiber samples were prepared as stated in the text, then 5 μL samples pipetted on to the grids, wicked off after 1 min, washed with water and uranyl acetate (5 μL) stain added for 45 s before being wicked off and the grid left to dry before imaging. Grids for cryo-TEM were glow discharged before insertion into the Vitrobot (FEI Company) (humidity was set to 100%, blotting time 1 s, adding 5 μL of sample prior to plunging into liquid ethane. Grids were then transferred to a cryo-holder (Gatan, Inc.).

X-ray Fiber Diffraction. Aligned samples were formed by suspending 10 μL of peptide samples between two wax-tipped capillary tubes, placing in a sealed Petri dish and allowing to dry by evaporation at room temperature. The resultant stalk of aligned peptide fibers was mounted and aligned on a goniometer. Diffraction data were collected using a rotating Cu Kα source Rigaku rotating anode with Saturn CCD detector with specimen to detector distances of 100 mm and

DOI: 10.1021/jacs.5b03973
J. Am. Chem. Soc. 2015, 137, 10554–10562

exposure times of 10−200 s. Fiber diffraction patterns were processed and analyzed using CLEARER.[34]

Single Crystal X-ray Diffraction. X-ray diffraction data were collected at the Diamond Light Source on station I02 using radiation of wavelength initially at 1.70 Å and then at 0.9795 Å. Data were processed with XDS.[35] The structure of CC-Hex-IL was solved by SHELX[36] using the 1.7 Å data set and single anomalous diffraction from the iodine atoms of iodophenylalanine side chains incorporated within the sequence. The final refined structure was obtained by subsequent iterative model building with the program COOT,[37] and refinement with REFMAC.[38]

DPH-Binding Experiments. Binding experiments were carried out in a well-plate format in PBS buffer at 25 °C, and at a steady DPH concentration of 1 μM. Peptide concentrations varied from 10 to 150 μM in order to record saturation binding curves. The mixtures of peptides and DPH were left to equilibrate for 2 h at 25 °C and under gentle shaking. Fluorescence spectra were then recorded in a range of 380−600 nm with λ_{ex} = 350 nm using a Clariostar plate reader from BMG Labtech. Saturation binding curves were generated from DPH fluorescence at 455 nm and were normalized to facilitate direct comparison.

■ ASSOCIATED CONTENT

Supporting Information

The Supporting Information is available free of charge on the ACS Publications website at DOI: 10.1021/jacs.5b03973.

Additional figures and tables, experimental details, methods, and characterization data (PDF)

■ AUTHOR INFORMATION

Corresponding Author

*d.n.woolfson@bristol.ac.uk

Author Contributions

$^{\nabla}$T.H.S. and F. T. contributed equally.

Notes

The authors declare no competing financial interest.

■ ACKNOWLEDGMENTS

N.C.B. thanks the EPSRC-funded Bristol Centre for Functional Nanomaterials Centre for Doctoral Training for a postgraduate scholarship (EP/G036780/1). F.T. and D.N.W. thank the Leverhulme Trust for funding (RPG-2012-536). D.N.W. holds a Royal Society Wolfson Research Merit Award. We thank the Chemistry Electron Microscopy Unit and the Wolfson Bioimaging Facility at the University of Bristol, and the Electron Microscopy Unit at Leiden University Medical Centre for access to the equipment and facilities and Jonathan Jones and Judith Mantell for technical assistance. Finally, we thank Vince Conticello for helpful discussions.

■ REFERENCES

(1) Hamley, I. W. *Angew. Chem., Int. Ed.* **2014**, *53*, 6866.

(2) Boyle, A. L.; Woolfson, D. N. In *Supramolecular Chemistry: From Molecules to Nanomaterials*; Steed, J. W., Gale, P. A., Eds.; John Wiley & Sons, Ltd: New York, 2012; p 1639.

(3) Woolfson, D. N.; Mahmoud, Z. N. *Chem. Soc. Rev.* **2010**, *39*, 3464.

(4) Seabra, A. B.; Durán, N. *Peptides* **2013**, *39*, 47.

(5) MacFarlane, A. A.; Orriss, G.; Okun, N.; Meier, M.; Klonisch, T.; Khajehpour, M.; Stetefeld, J. *PLoS One* **2012**, *7*, e48130.

(6) Burton, A. J.; Thomas, F.; Agnew, C.; Hudson, K. L.; Halford, S. E.; Brady, R. L.; Woolfson, D. N. *J. Am. Chem. Soc.* **2013**, *135*, 12524.

(7) Reches, M.; Gazit, E. *Science* **2003**, *300*, 625.

(8) Ghadiri, M. R.; Granja, J. R.; Milligan, R. A.; McRee, D. E.; Khazanovich, N. *Nature* **1993**, *366*, 324.

(9) Hartgerink, J. D.; Granja, J. R.; Milligan, R. A.; Ghadiri, M. R. *J. Am. Chem. Soc.* **1996**, *118*, 43.

(10) Pandya, M. J.; Spooner, G. M.; Sunde, M.; Thorpe, J. R.; Rodger, A.; Woolfson, D. N. *Biochemistry* **2000**, *39*, 8728.

(11) Dong, H.; Paramonov, S. E.; Hartgerink, J. D. *J. Am. Chem. Soc.* **2008**, *130*, 13691.

(12) Zimenkov, Y.; Conticello, V. P.; Guo, L.; Thiyagarajan, P. *Tetrahedron* **2004**, *60*, 7237.

(13) Sharp, T. H.; Bruning, M.; Mantell, J.; Sessions, R. B.; Thomson, A. R.; Zaccai, N. R.; Brady, R. L.; Verkade, P.; Woolfson, D. N. *Proc. Natl. Acad. Sci. U. S. A.* **2012**, *109*, 13266.

(14) Woolfson, D. N.; Bartlett, G. J.; Bruning, M.; Thomson, A. R. *Curr. Opin. Struct. Biol.* **2012**, *22*, 432.

(15) Potekhin, S. A.; Melnik, T. N.; Popov, V.; Lanina, N. F.; Vazina, A. A.; Rigler, P.; Verdini, A. S.; Corradin, G.; Kajava, A. V. *Chem. Biol.* **2001**, *8*, 1025.

(16) Hume, J.; Sun, J.; Jacquet, R.; Renfrew, P. D.; Martin, J. A.; Bonneau, R.; Gilchrist, M. L.; Montclare, J. K. *Biomacromolecules* **2014**, *15*, 3503.

(17) Xu, C.; Liu, R.; Mehta, A. K.; Guerrero-Ferreira, R. C.; Wright, E. R.; Dunin-Horkawicz, S.; Morris, K.; Serpell, L. C.; Zuo, X.; Wall, J. S.; Conticello, V. P. *J. Am. Chem. Soc.* **2013**, *135*, 15565.

(18) Fletcher, J. M.; Boyle, A. L.; Bruning, M.; Bartlett, G. J.; Vincent, T. L.; Zaccai, N. R.; Armstrong, C. T.; Bromley, E. H. C.; Booth, P. J.; Brady, R. L.; Thomson, A. R.; Woolfson, D. N. *ACS Synth. Biol.* **2012**, *1*, 240.

(19) Bromley, E. H. C.; Sessions, R. B.; Thomson, A. R.; Woolfson, D. N. *J. Am. Chem. Soc.* **2009**, *131*, 928.

(20) Thomas, F.; Boyle, A. L.; Burton, A. J.; Woolfson, D. N. *J. Am. Chem. Soc.* **2013**, *135*, 5161.

(21) Nautiyal, S.; Alber, T. *Protein Sci.* **1999**, *8*, 84.

(22) Zaccai, N. R.; Chi, B.; Thomson, A. R.; Boyle, A. L.; Bartlett, G. J.; Bruning, M.; Linden, N.; Sessions, R. B.; Booth, P. J.; Brady, R. L.; Woolfson, D. N. *Nat. Chem. Biol.* **2011**, *7*, 935.

(23) Thomson, A. R.; Wood, C. W.; Burton, A. J.; Bartlett, G. J.; Sessions, R. B.; Brady, R. L.; Woolfson, D. N. *Science* **2014**, *346*, 485.

(24) Yoshizumi, A.; Fletcher, J. M.; Yu, Z.; Persikov, A. V.; Bartlett, G. J.; Boyle, A. L.; Vincent, T. L.; Woolfson, D. N.; Brodsky, B. *J. Biol. Chem.* **2011**, *286*, 17512.

(25) Fletcher, J. M.; Harniman, R. L.; Barnes, F. R. H.; Boyle, A. L.; Collins, A.; Mantell, J.; Sharp, T. H.; Antognozzi, M.; Booth, P. J.; Linden, N.; Miles, M. J.; Sessions, R. B.; Verkade, P.; Woolfson, D. N. *Science* **2013**, *340*, 595.

(26) Papapostolou, D.; Smith, A. M.; Atkins, E. D. T.; Oliver, S. J.; Ryadnov, M. G.; Serpell, L. C.; Woolfson, D. N. *Proc. Natl. Acad. Sci. U. S. A.* **2007**, *104*, 10853.

(27) Crick, F. *Acta Crystallogr.* **1953**, *6*, 689.

(28) Papapostolou, D.; Bromley, E. H. C.; Bano, C.; Woolfson, D. N. *J. Am. Chem. Soc.* **2008**, *130*, 5124.

(29) Stewart, M. *J. Electron Microsc. Tech.* **1988**, *9*, 325.

(30) Wood, C. W.; Bruning, M.; Ibarra, A. Á.; Bartlett, G. J.; Thomson, A. R.; Sessions, R. B.; Brady, R. L.; Woolfson, D. N. *Bioinformatics* **2014**, *30*, 3029.

(31) Jacobson, K.; Papahadjopoulos, D. *Biochemistry* **1975**, *14*, 152.

(32) Jahnig, F. *Proc. Natl. Acad. Sci. U. S. A.* **1979**, *76*, 6361.

(33) Bromley, E. H. C.; Channon, K. J.; King, P. J. S.; Mahmoud, Z. N.; Banwell, E. F.; Butler, M. F.; Crump, M. P.; Dafforn, T. R.; Hicks, M. R.; Hirst, J. D.; Rodger, A.; Woolfson, D. N. *Biophys. J.* **2010**, *98*, 1668.

(34) Sumner Makin, O.; Sikorski, P.; Serpell, L. C. *J. Appl. Crystallogr.* **2007**, *40*, 966.

(35) Kabsch, W. *Acta Crystallogr., Sect. D: Biol. Crystallogr.* **2010**, *66*, 125.

(36) Sheldrick, G. *Acta Crystallogr., Sect. A: Found. Crystallogr.* **2008**, *64*, 112.

(37) Emsley, P.; Cowtan, K. *Acta Crystallogr., Sect. D: Biol. Crystallogr.* **2004**, *60*, 2126.

(38) Murshudov, G. N.; Vagin, A. A.; Dodson, E. J. *Acta Crystallogr., Sect. D: Biol. Crystallogr.* **1997**, *53*, 240.

DOI: 10.1021/jacs.5b03973
J. Am. Chem. Soc. 2015, 137, 10554−10562